METHOD OF LINES
FOR THE INCOMPRESSIBLE
NAVIER-STOKES EQUATIONS
IN THE STREAM-FUNCTION
FORMULATION

ZBIGNIEW KOSMA

Institute of Applied Mechanics,
Radom University of Technology,
Krasickiego 54, 26-600 Radom, Poland
zkosma@pr.radom.pl

Abstract: The aim of this paper is to simulate the laminar motion of viscous incompressible fluid and the transition between the laminar and the turbulent state in simply connected domains. The developed numerical algorithms are based on the solution of an initial-boundary value problem for the full incompressible Navier-Stokes equations, written in the form of a fourth-order equation for the stream function. The spatial derivatives and the boundary conditions are discretized on uniform grids by means of sixth-order compact schemes together with fourth-order finite-difference formulas, while the continuity of the time variable is preserved. The resulting system of ordinary differential equations has been integrated using the backward-differentiation predictor-corrector method. The efficiency of the numerical algorithms is demonstrated by solving two problems of viscous liquid plane flows in a square driven cavity and a backward-facing step. Calculations for the cavity flow configuration have been obtained for Reynolds numbers ranging from $\mathrm{Re} = 100$ to $\mathrm{Re} = 30\,000$ on uniform 50×50 and 100×100 grids. Calculations for the backward-facing step have been made for $\mathrm{Re} \leq 3000$ with channel lengths, L, within the range 10–30, on $30L \times 30$ uniform grids. The computed stream-function contours and velocity fields have been compared with numerical results reported in the literature.

Keywords: Navier-Stokes equation, stream-function formulation, method of lines, compact schemes, driven cavity problem, backward-facing step flow

1. Navier-Stokes equations in the stream-function form

The problem of determination of the unsteady plane motion of viscous incompressible fluid can be formulated mathematically as an initial-boundary value problem for the fourth-order equation which governs the stream-function distribution [1, 2]:

$$\frac{\partial \vec{\nabla}^2 \psi}{\partial t} + \frac{\partial \vec{\nabla}^2 \psi}{\partial x} \frac{\partial \psi}{\partial y} - \frac{\partial \vec{\nabla}^2 \psi}{\partial y} \frac{\partial \psi}{\partial x} = \frac{1}{\mathrm{Re}} \vec{\nabla}^4 \psi, \tag{1}$$

where Re denotes the Reynolds number, and $\vec{\nabla}^2$ is the Laplace operator. The governing Equation (1) was transformed into a dimensionless form with appropriate normalizations.

The simplicity of formulation of Equation (1) lies in the fact that the continuity equation is satisfied automatically, and then the boundary conditions for the stream-function in simply connected domains are explicitly specified by given velocity distributions. A disadvantage of this formulation is the high order of Equation (1).

The velocity components are defined as:

$$u = \frac{\partial \psi}{\partial y}, \qquad v = -\frac{\partial \psi}{\partial x}, \tag{2}$$

and vorticity, $\omega = \partial v / \partial x - \partial u / \partial y$, satisfies the equation $\omega = -\vec{\nabla}^2 \psi$.

2. Numerical approach

Approximations of all the derivatives with respect to spatial independent variables x, y occuring in Equation (1) have been performed using compact finite difference schemes [3], defined as generalizations of the classical Padé schemes.

The results of the theory of these schemes, applied to an auxiliary discrete function, φ_k, of a real variable ξ_k:

$$\varphi_k = \varphi(\xi_k), \qquad \xi_k = \xi_0 + kh \quad (k = 0, 1, \ldots, N), \tag{3}$$

yield the following sixth-order tridiagonal approximations of the first derivatives:

$$\frac{1}{3}\varphi'_{k-1} + \varphi'_k + \frac{1}{3}\varphi'_{k+1} = \frac{14}{9}\frac{\varphi_{k+1} - \varphi_{k-1}}{2h} + \frac{1}{9}\frac{\varphi_{k+2} - \varphi_{k-2}}{4h}, \tag{4}$$
$$(k = 2, 3, \ldots, N-2),$$

and a similar three-point formula for the second derivatives:

$$\frac{2}{11}\varphi''_{k-1} + \varphi''_k + \frac{2}{11}\varphi''_{k+1} = \frac{12}{11}\frac{\varphi_{k+1} - 2\varphi_k + \varphi_{k-1}}{h^2} + \frac{3}{11}\frac{\varphi_{k+2} - 2\varphi_k + \varphi_{k-2}}{4h^2}, \tag{5}$$
$$(k = 2, 3, \ldots, N-2).$$

In practice, the non-periodic boundary formulation for the first derivatives is given by the following third- and fourth-order relations:

$$\varphi'_0 + 2\varphi'_1 = \frac{1}{h}\left(-\frac{5}{2}\varphi_0 + 2\varphi_1 + \frac{1}{2}\varphi_2\right) \quad (k = 0),$$
$$\frac{1}{4}\varphi'_0 + \varphi'_1 + \frac{1}{4}\varphi'_2 = \frac{3}{4h}\left(\varphi_2 - \varphi_0\right) \quad (k = 1),$$
$$\frac{1}{4}\varphi'_{N-2} + \varphi'_{N-1} + \frac{1}{4}\varphi'_N = \frac{3}{4h}\left(\varphi_N - \varphi_{N-2}\right) \quad (k = N-1), \tag{6}$$
$$2\varphi'_{N-1} + \varphi'_N = \frac{1}{h}\left(-\frac{1}{2}\varphi_{N-2} - 2\varphi_{N-1} + \frac{5}{2}\varphi_N\right) \quad (k = N),$$

while the non-periodic boundary formulation for the second derivatives is taken in the following form:

$$
\begin{aligned}
\varphi_0'' + 11\varphi_1'' &= \frac{1}{h^2}\Big(13\varphi_0 - 27\varphi_1 + 15\varphi_2 - \varphi_3\Big) \quad (k=0), \\
\frac{1}{10}\varphi_0'' + \varphi_1'' + \frac{1}{10}\varphi_2'' &= \frac{6}{5h^2}\Big(\varphi_2 - 2\varphi_1 + \varphi_0\Big) \quad (k=1), \\
\frac{1}{10}\varphi_{N-2}'' + \varphi_{N-1}'' + \frac{1}{10}\varphi_N'' &= \frac{5}{6h^2}\Big(\varphi_{N-2} - 2\varphi_{N-1} + \varphi_N\Big) \quad (k=N-1), \\
11\varphi_{N-1}'' + \varphi_N'' &= \frac{1}{h^2}\Big(-\varphi_{N-3} + 15\varphi_{N-2} - 27\varphi_{N-1} + 13\varphi_N\Big) \quad (k=N).
\end{aligned}
\tag{7}
$$

A set of formulas for determining the spatial derivatives of the $\vec{\nabla}^2\psi$ function can be obtained directly from Equations (4)–(7) by replacing φ_k with $\big(\vec{\nabla}^2\psi\big)\big|_k$.

In order to solve the initial-boundary value problem for Equation (1), we cover the relevant quadratic or rectangular domain in the $x \times y$ plane with a grid system defined by:

$$
\begin{aligned}
x &= x_0 + kh \quad (k=0,1,\ldots,K), \\
y &= y_0 + lh \quad (l=0,1,\ldots,L),
\end{aligned}
\tag{8}
$$

where h is the same spacing of the grid in the x and y directions.

Using central differences [4], the Laplacian operator $\vec{\nabla}^2$ in the non-stationary term $\partial\vec{\nabla}^2\psi/\partial t$ can be replaced with its finite difference approximations:

$$
\begin{aligned}
\big(\vec{\nabla}^2\psi\big)_{i,j} = \frac{1}{12h^2}\Big(&-\psi_{i-2,j} - \psi_{i+2,j} - \psi_{i,j-2} - \psi_{i,j+2} + \\
&+16\psi_{i-1,j} + 16\psi_{i+1,j} + 16\psi_{i,j-1} + 16\psi_{i,j+1} - 60\psi_{i,j}\Big) + O(h^4),
\end{aligned}
\tag{9}
$$

at interior grid points $i = 2,3,\ldots,K-2$, $j = 2,3,\ldots,L-2$. Systems of ordinary differential equations can thus be obtained in these nodes of the assumed uniform computational grid (8):

$$
\begin{aligned}
a_{i-2,j}\dot{\psi}_{i-2,j} + a_{i+2,j}\dot{\psi}_{i+2,j} + a_{i,j-2}\dot{\psi}_{i,j-2} + a_{i,j+2}\dot{\psi}_{i,j+2} + \\
+a_{i-1,j}\dot{\psi}_{i-1,j} + a_{i+1,j}\dot{\psi}_{i+1,j} + a_{i,j-1}\dot{\psi}_{i,j-1} + a_{i,j+1}\dot{\psi}_{i,j+1} + a_{i,j}\dot{\psi}_{i,j} = \tilde{f}(\psi_{k,l}),
\end{aligned}
\tag{10}
$$

where the dots indicate first derivatives with respect to time, being the only continuous independent variable, and coefficients $a_{i,j}$ are constant. The right-hand side, $\tilde{f}(\psi_{k,l})$, contains approximated values of the discretized convective and diffusive terms of Equation (1), while indices k, l are mesh points (8).

The lacking equations along the $i=1$, $i=K-1$, $j=1$ and $j=L-1$ lines can be obtained from boundary conditions involving a constant and specified stream-function and its normal derivatives on the boundaries. Based on the following finite-differences expressions [4]:

$$
\begin{aligned}
\varphi_0' &= \frac{1}{12h}\Big(-25\varphi_0 + 48\varphi_1 - 36\varphi_2 + 16\varphi_3 - 3\varphi_4\Big) + O(h^4), \\
\varphi_N' &= \frac{1}{12h}\Big(3\varphi_{N-4} - 16\varphi_{N-3} + 36\varphi_{N-2} - 48\varphi_{N-1} + 25\varphi_N\Big) + O(h^4),
\end{aligned}
\tag{11}
$$

we can find additional relationships:

$$
\begin{aligned}
\dot{\psi}_{1,j} &= \frac{3}{4}\dot{\psi}_{2,j} - \frac{1}{3}\dot{\psi}_{3,j} + \frac{1}{16}\dot{\psi}_{4,j}, \\
\dot{\psi}_{K-1,j} &= \frac{3}{4}\dot{\psi}_{K-2,j} - \frac{1}{3}\dot{\psi}_{K-3,j} + \frac{1}{16}\dot{\psi}_{K-4,j}, \\
\dot{\psi}_{i,1} &= \frac{3}{4}\dot{\psi}_{i,2} - \frac{1}{3}\dot{\psi}_{i,3} + \frac{1}{16}\dot{\psi}_{i,4}, \\
\dot{\psi}_{i,L-1} &= \frac{3}{4}\dot{\psi}_{i,L-2} - \frac{1}{3}\dot{\psi}_{i,L-3} + \frac{1}{16}\dot{\psi}_{i,L-4}.
\end{aligned}
\tag{12}
$$

Hence we can obtain fourth-order accurate difference approximations to $\left(\vec{\nabla}^2\dot{\psi}\right)_{i,j}$ with mesh points values of $i = 2,\ 3,\ K-3,\ K-2$, $j = 2,\ 3,\ L-3,\ L-2$, and the corresponding Equations (10) at these points, for example:

$$
\begin{aligned}
\frac{32}{3}\dot{\psi}_{3,2} + \frac{32}{3}\dot{\psi}_{2,3} - 36\dot{\psi}_{2,2} &= \tilde{f}(\psi_{k,l}), \\
\frac{61}{4}\dot{\psi}_{2,2} + \frac{255}{16}\dot{\psi}_{4,2} - \dot{\psi}_{5,2} + \frac{32}{3}\dot{\psi}_{3,3} - \left(18 + \frac{89}{3}\right)\dot{\psi}_{3,2} &= \tilde{f}(\psi_{k,l}), \\
\frac{61}{4}\dot{\psi}_{2,3} + \frac{255}{16}\dot{\psi}_{4,3} - \dot{\psi}_{5,3} + \frac{61}{4}\dot{\psi}_{3,2} + \frac{255}{16}\dot{\psi}_{3,4} - \dot{\psi}_{3,5} - 2\frac{89}{3}\dot{\psi}_{3,3} &= \tilde{f}(\psi_{k,l}).
\end{aligned}
\tag{13}
$$

The modified system of linear algebraic equations (10) with coefficients determined from Equations (9) and (13) for the time derivatives can be easily solved by means of the over-relaxation Gauss-Seidel method [4] and leads to a system of ordinary differential equations in the Cauchy form (a method of lines approach):

$$
\dot{\psi}_{i,j} = f(\psi_{k,l}).
\tag{14}
$$

The obtained initial value problem for the system of ordinary differential equations (14) is integrated using the two-step backward-differentiation predictor-corrector method [5, 6].

Considering an initial value problem for an unknown function $\varphi(t)$:

$$
\begin{aligned}
\frac{\mathrm{d}\varphi}{\mathrm{d}t} &= f(t,\varphi), \quad \varphi = \varphi(t), \\
\varphi(0) &= \varphi_0, \quad t \in [0,T],
\end{aligned}
\tag{15}
$$

for this particular case becomes:

predictor

$$
\varphi_{n+1}^{(0)} = \varphi_{n-1} + 2\Delta t\, f(t_n,\varphi_n),
\tag{16}
$$

corrector

$$
\varphi_{n+1}^{(q+1)} = \frac{1}{3}\left[(4\varphi_n - \varphi_{n-1}) + 2\Delta t\, f(t_{n+1},\varphi_{n+1}^{(q)})\right] \quad (q = 0,1,\dots).
\tag{17}
$$

BDF-methods are currently in common use for stiff equations. The right-hand sides in Equations (16) and (17) are calculated only once at each step of integration, which allows one to decrease the calculation time. The 2-step BDF-formula (17) is stable in all the left conformal half-planes of the corresponding characteristic equation.

Another numerical scheme for incompressible viscous flow, formulated as Equation (1) for the stream-function, was proposed in [7]. In this paper the biharmonic

equation is discretized with a compact scheme and the advection of vorticity is implemented with a high-resolution central scheme.

3. The driven cavity problem

3.1. Computational domain and boundary conditions

Let us consider as the first example of the developed method the driven cavity flow shown in Figure 1, containing water in contact with a steady air flow over its surface. In this case, the stream function, ψ, has to fulfil the following boundary conditions:

$$\psi(0,y) = \psi(1,y) = \psi(x,0) = \psi(x,1) = 0,$$
$$\psi_x(0,y) = \psi_x(1,y) = \psi_y(x,0) = 0, \tag{18}$$
$$\psi_y(x,1) = 1.$$
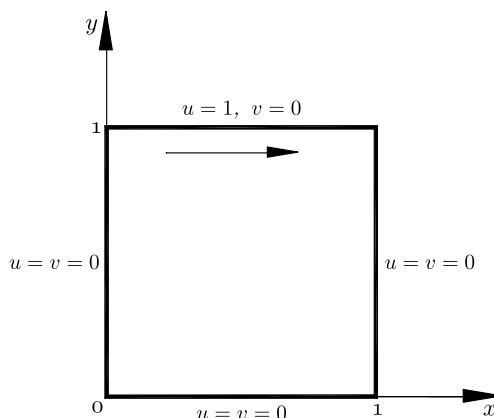
Figure 1. The driven cavity problem: geometry and boundary conditions

Cavity flows have been frequently employed to test the accuracy of Navier-Stokes solvers [7–46]. Numerical simulation of viscous incompressible fluid motion in a square cavity is not only important technologically, it is also of great scientific interest as it displays most fluid mechanical phenomena in a simple geometrical setting. Multiple regions of re-circulation, non-uniqueness, transition and turbulence occur naturally and can be studied in the same domain.

3.2. Numerical results

The quadratic domain in the x-y plane (Figure 1) was covered by a grid system, $N \times N$, defined by $x = ih$, $y = jh$ $(i,j = 0,1,\ldots,N)$, where $h = 1/N$.

Several preliminary tests had been done [47–49] on 50×50 and 100×100 grids according to the algorithm with second- and fourth-order approximations of $\vec{\nabla}^2 \psi$ in the time-dependent term in connection with fourth-order approximations of the spatial derivatives derived from the theory of cubic spline functions. The proposed method seemed to be quite promising as an incompressible Navier-Stokes solver for laminar as well as turbulent flows, taking into account that the transition from laminar to turbulent flows occurs about $\mathrm{Re} \approx 8000$ [38, 41].

The computed streamlines on the 50×50 and 100×100 grids obtained according to the present algorithm for Reynolds numbers ranging from $\mathrm{Re} = 100$ to $\mathrm{Re} = 30\,000$ are presented in Figures 2–6. Converged solutions for $\mathrm{Re} = 100$ with the assumption of $\psi_0 = 0$ were obtained and then used as the initial conditions for the case of $\mathrm{Re} = 400$, and so forth. The time steps were taken as $\Delta t = 10^{-3}$ for the 50×50 grid and $\Delta t = 10^{-4}$ for the 100×100 grid, while iterations for the solution of the system of Equations (10) and the backward-differentiation corrector (17) were repeated until an accuracy of $[1 \cdot 10^{-11}, 1 \cdot 10^{-7}]$ was achieved. The process of integration was terminated after arriving at the steady state ($\mathrm{Re} \leq 10\,000$), defined as:

$$\max \left| \Delta \big(\mathrm{Re}\, \dot{\psi}_{i,j} \big) \right| \leq \delta, \quad \delta \in [1 \cdot 10^{-9}, 1 \cdot 10^{-7}]. \tag{19}$$

The effect of the spatial grid's size on the accuracy of the time-dependent solution has also been studied. It was possible to compute steady solutions for Reynolds numbers up to 10 000, but the results on the 50×50 grid at $\mathrm{Re} > 1000$ differed considerably from results reported in the literature [7–45]. Steady states were reached after about $20\,000$–$50\,000$ time steps. As confirmed in [15], an unstable solution at $\mathrm{Re} = 30\,000$ was also found on the 100×100 grid and in this case the computations were performed until a specified number of iterations (equal to $20\,000$) was reached.

Figures 2–6 show how flows in the cavity depend on the Reynolds number. The flow configuration is characterized by the locations of the centres and sizes of the main vortex and the secondary vortices. The primary vortex moves down to the centre of the cavity as the Reynolds number increases. It is getting stronger and its location becomes virtually invariant for $\mathrm{Re} \geq 5000$ [15]. Small eddies develop in the vicinity of the two lower corners and in the upper right corner, and their centres also move very slowly towards the cavity's centre with the increase of Re. The interaction of these eddying motions with the mean shear-driven flow eventually leads to a turbulence, as small eddies are unstable and the strength of the primary eddy at the centre of the cavity varies in time. All the secondary vortices on the 100×100 grid for the steady state solutions are shown in Figures 7–12, where velocity vectors are plotted with vector length proportional to the magnitude of velocity.

3.3. Discussion of results

The driven square cavity flow is a good benchmark problem as it offers a deceptively simple model on which numerical techniques may be examined and very accurate numerical results are available for comparison. The computed stream-function contours and distributions of velocity components, appearance of vortices in the flow field and the observed locations of primary, secondary and additional corner vortices are compatible with the numerical results reported in the literature [7–46]. Especially the stream-function contours are graphically comparable with the well-known figures obtained by Ghia *et al.* [9]. The 100×100 grid is found to be good enough to capture the flow details including the tertiary vortices up to $\mathrm{Re} = 10\,000$.

Figures 13–20 show the computed profiles concerning the u velocity component on the vertical centreline of the cavity ($x = 0.5$), the v velocity component along the horizontal centreline of the cavity ($y = 0.5$) and their comparisons with the
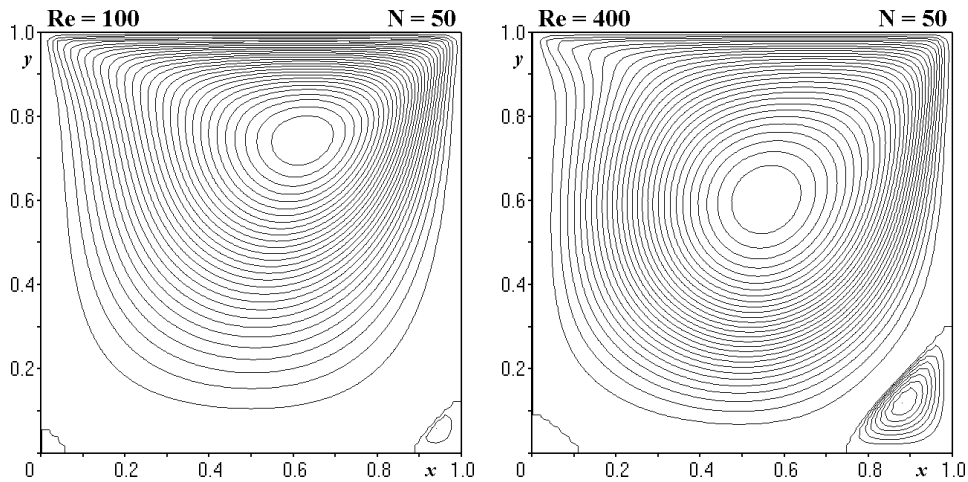
Figure 2. Stream-function contours: Re = 100 and 400, 50 × 50 grid

corresponding data from Ghia *et al.* [9]. It is worth noting that Ghia *et al.* used a 129 × 129 mesh at Re ≤ 3200 and a 257 × 257 mesh at Re ≥ 5000. Although we used 50 × 50 and 100 × 100 meshes, the accuracy of the solutions appears almost the same as those in the referenced paper. For the Reynolds numbers of 7500 and 10 000 the present method yields slightly higher extremal values of the velocity components since it is difficult to resolve the very thin boundary layer with a uniform grid, although the rate of this thinning is very slow for Re ≥ 5000.

The results indicate that with an increase of the Reynolds number the effect of viscosity is confined to a thin layer close to the solid boundaries. Another effect is that the local curvature of the resulting mean velocity profiles increases. In order to obtain additional detailed local flow characteristics for high Reynolds numbers (Re ≥ 10 000), very fine uniform or non-uniform meshes should be used [9, 13, 15, 16, 40, 42]. In [49] grids have been clustered near the walls using algebraic stretching functions.

4. Backward-facing step flow

4.1. Computational domain and boundary conditions

The second case considered is the motion of viscous liquid in a rectilinear two-dimensional backward-facing step (flow over a sudden expansion), the flow geometry of which is shown in Figure 21. The downstream channel was defined to have unit height. The step height and the height of the inlet region are the same. The length of the computational domain, L, was taken from the range 10–30 and increased with the Reynolds number. The co-ordinate system for describing locations in the channel is centred in the top corner and its axes are parallel to the channel sides. A parabolic velocity profile $u(y) = 24y(0.5 - y)$ for $0 \leq y \leq 0.5$ at the inlet and no-slip conditions on solid walls are prescribed. This produces a maximum inflow velocity of $u_{max} = 1.5$ and an average inflow velocity of $u_{ave} = 1.0$. At the outlet, the imposed boundary conditions also assumed a parallel flow and depended on the flow model. A parabolic velocity profile is also used for laminar flow, while for laminar-turbulent flow the $\partial \psi / \partial y$ derivative via an extrapolation formula is calculated and $\partial^2 \psi / \partial y^2 = 0$
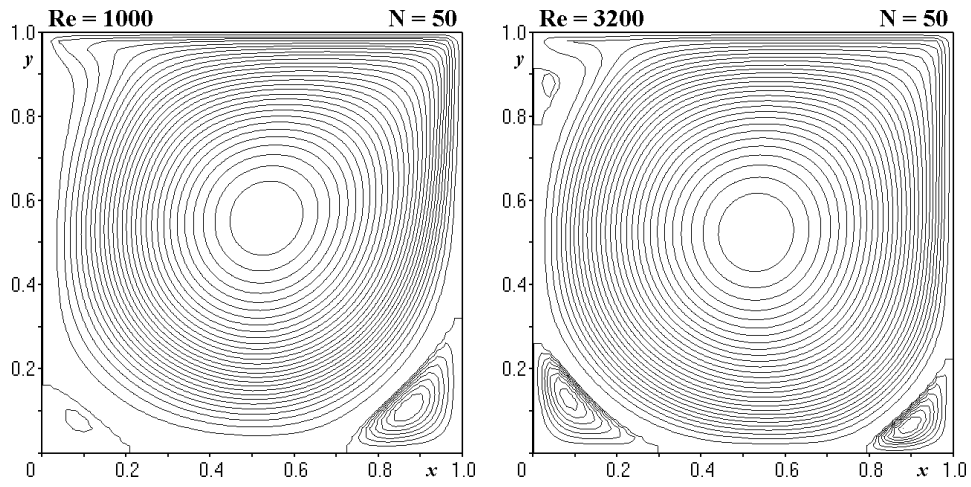
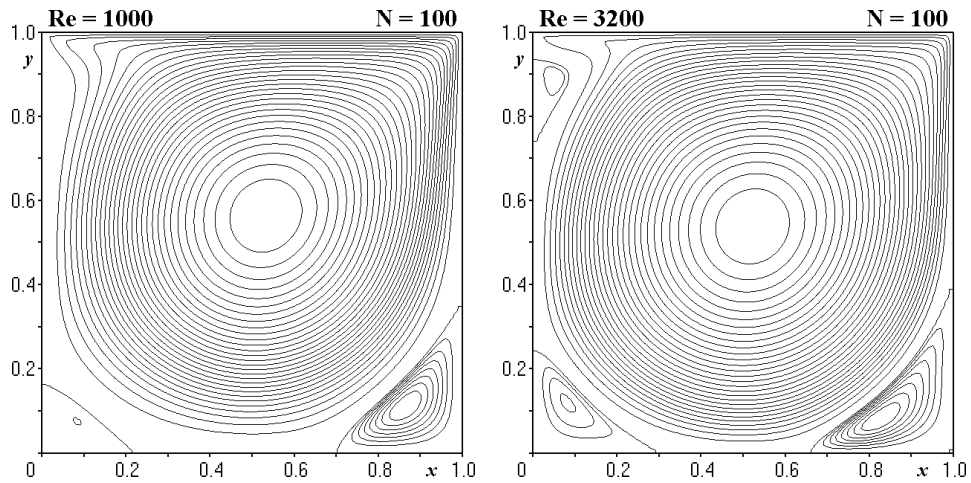**Figure 3.** Stream-function contours: Re = 1000 and 3200, 50 × 50 grid

Figure 4. Stream-function contours: Re = 1000 and 3200, 100 × 100 grid
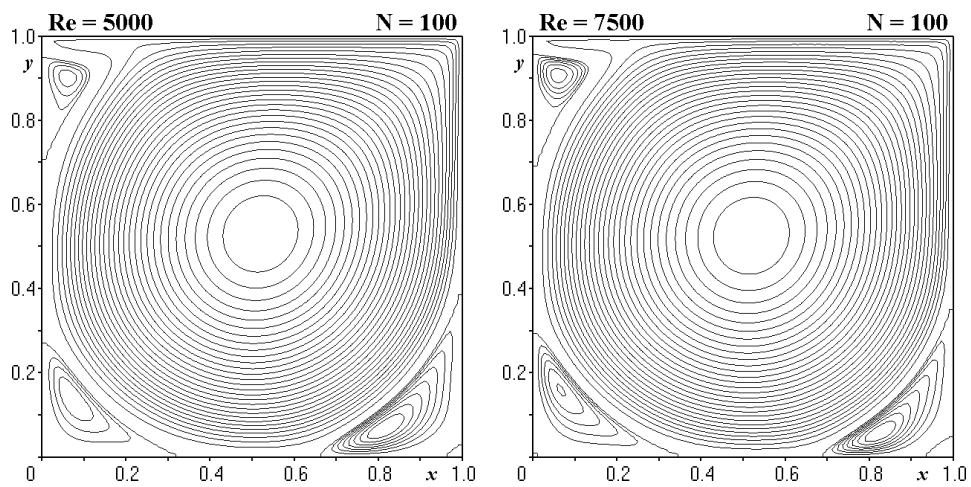

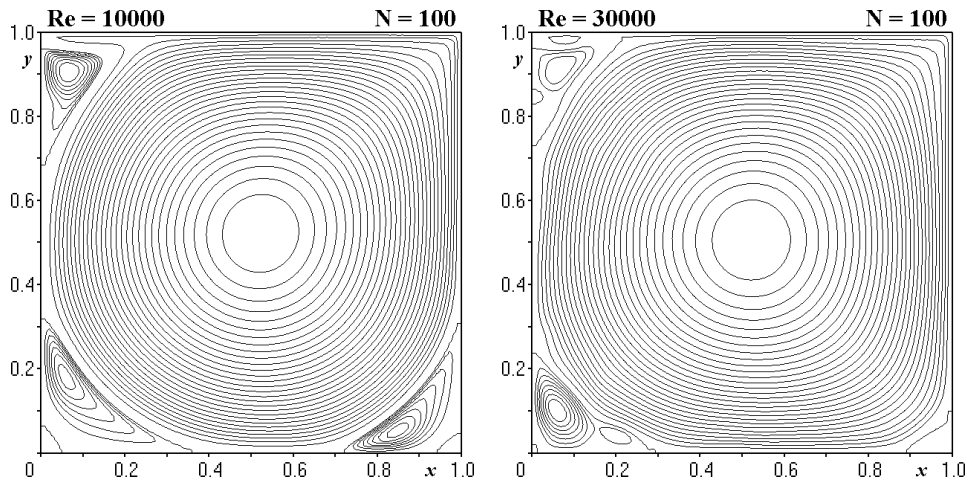**Figure 5.** Stream-function contours: Re = 5000 and 7500, 100 × 100 grid

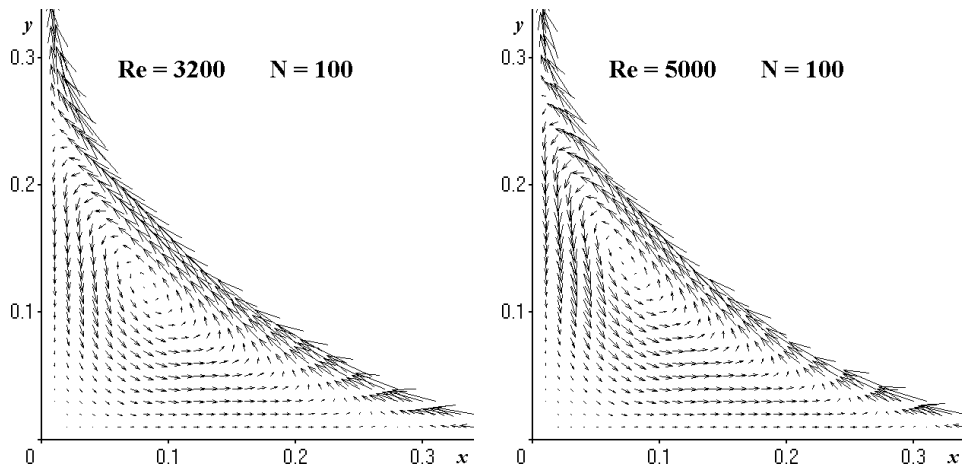**Figure 6.** Stream-function contours: Re = 10 000 and 30 000, 100 × 100 grid

Figure 7. Velocity distribution in the bottom left-hand corner: Re = 3200 and 5000
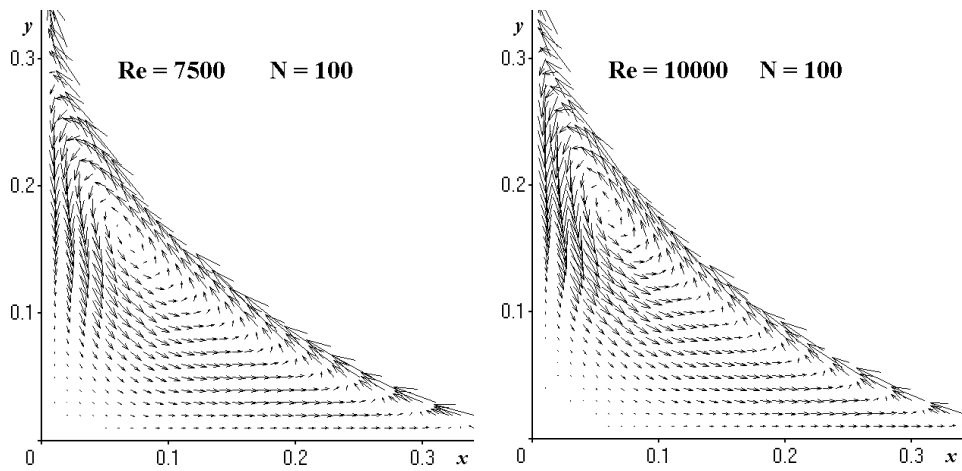
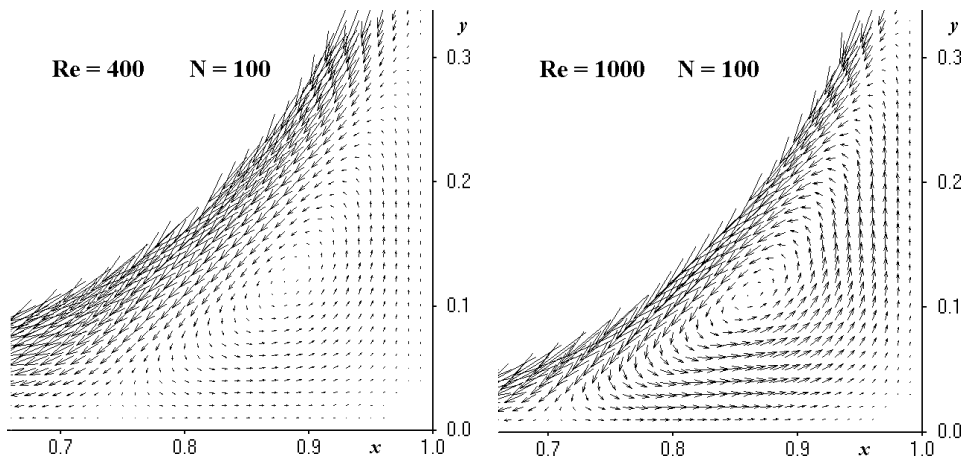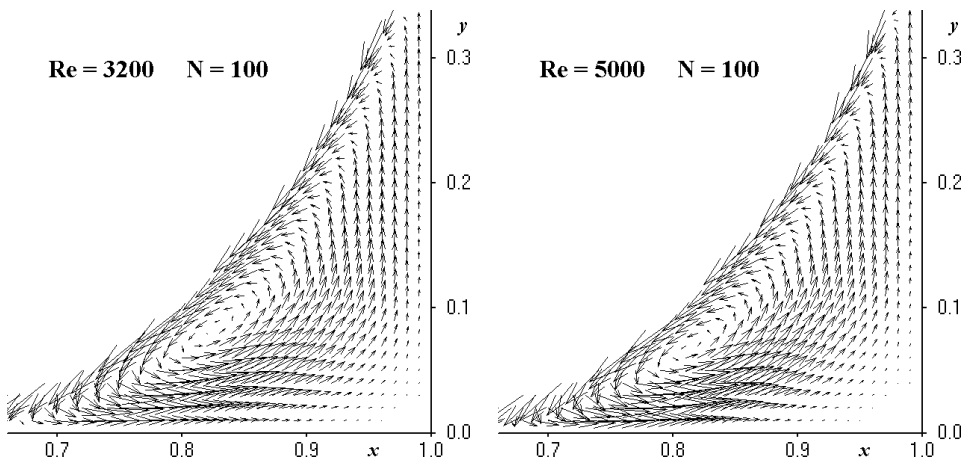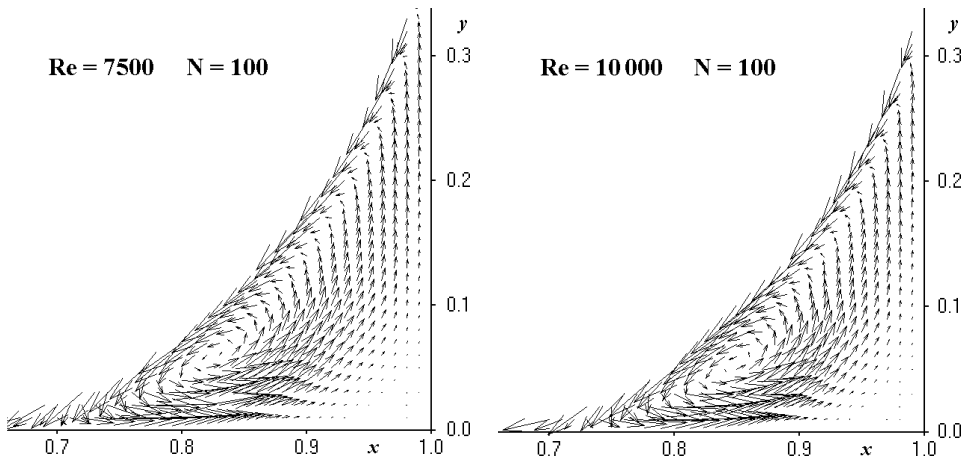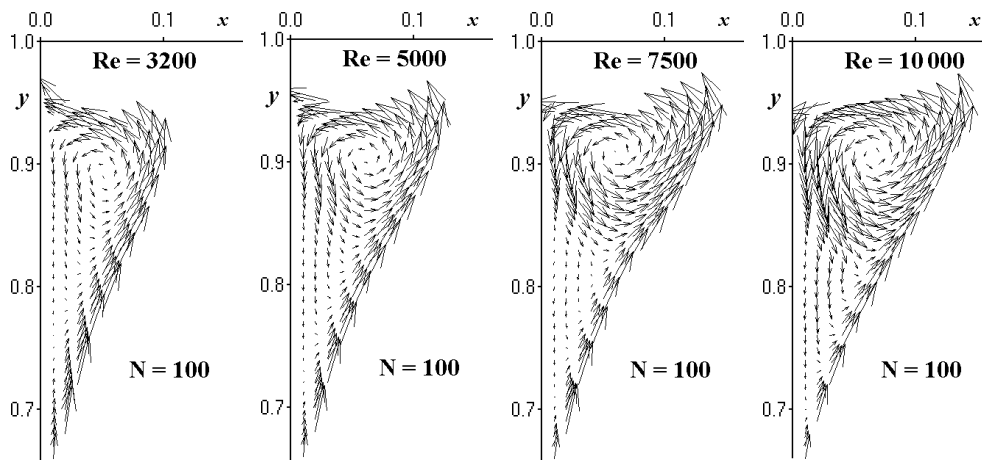**Figure 8.** Velocity distribution in the bottom left-hand corner: Re = 7500 and 10 000

Figure 9. Velocity distribution in the bottom right-hand corner: Re = 400 and 1000

Figure 10. Velocity distribution in the bottom right-hand corner: Re = 3200 and 5000

Figure 11. Velocity distribution in the bottom right-hand corner: Re = 7500 and 10 000

Figure 12. Velocity distribution in the upper right corner: $Re = 3200$, 5000, 7500 and 10 000

is postulated. Hence, boundary conditions for laminar flow correspond to those defined in the literature [19, 35, 49–73] and can be expressed in the following manner:

$$\psi = 0 \text{ for } y = -0.5, \ x \in [0, L],$$
$$\psi = 0 \text{ for } x = 0, \ y \in [-0.5, 0],$$
$$\psi = 2y^2(3 - 4y) \text{ for } x = 0, \ y \in [0, 0.5], \quad (20)$$
$$\psi = 0.25 + (3 - 4y^2)y/4 \text{ for } x = L, \ y \in [-0.5, 0.5],$$
$$\psi = 0.5 \text{ for } y = 0.5, \ x \in [0, L].$$
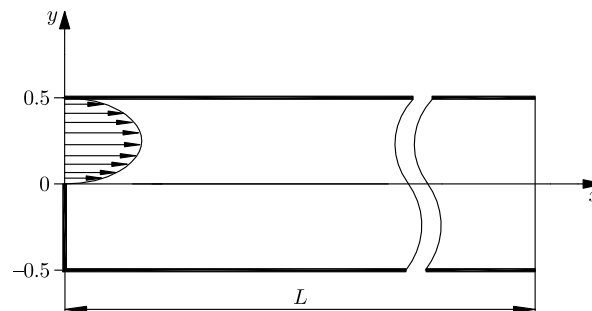
Figure 21. Geometry of the backward-facing step problem

Results of computations of viscous incompressible flows in a backward-facing geometry have been reported by many of authors [19, 28, 35, 49–73]. This simple configuration involves a few re-circulating flow regions (see Figure 22) and vortex-shedding phenomena, experimentally studied by Armaly *et al.* [50] for the flow of air. Unfortunately, the three-dimensional effects in the channel become significant for $Re > 400$, which makes comparison of the measurements with the two-dimensional simulations less than satisfactory. However, the laminar ($Re < 1200$), transitional ($1200 < Re < 6600$) and turbulent ($Re > 6600$) zones of the flow can be clearly identified from the measurements.
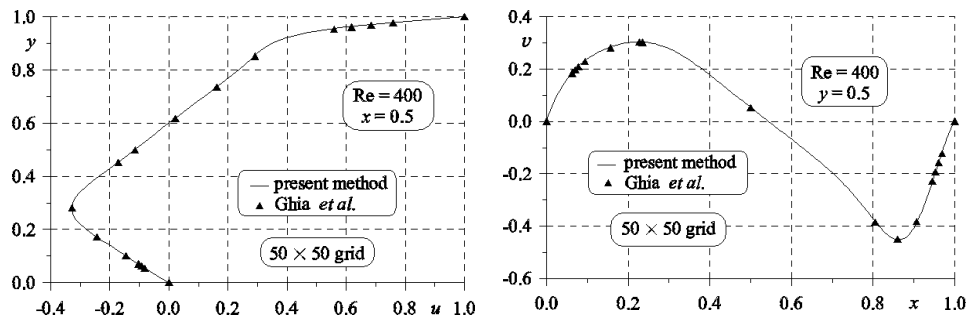
Figure 13. Distributions of the x and y components of velocity on the centrelines
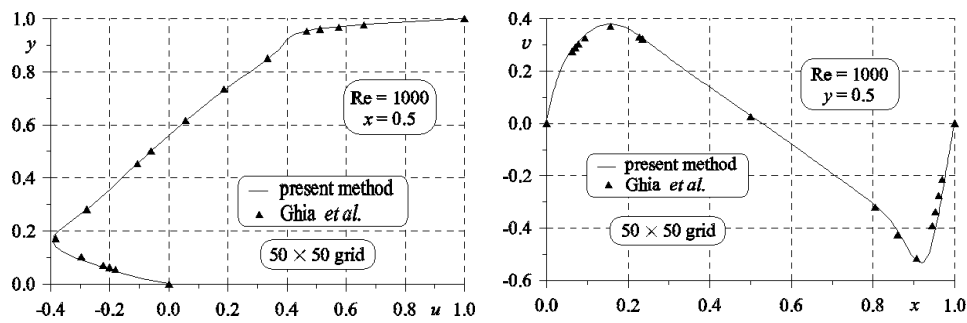of the cavity at $Re = 400$, the 50×50 grid

Figure 14. Distributions of the x and y components of velocity on the centrelines
of the cavity at $Re = 1000$, the 50×50 grid
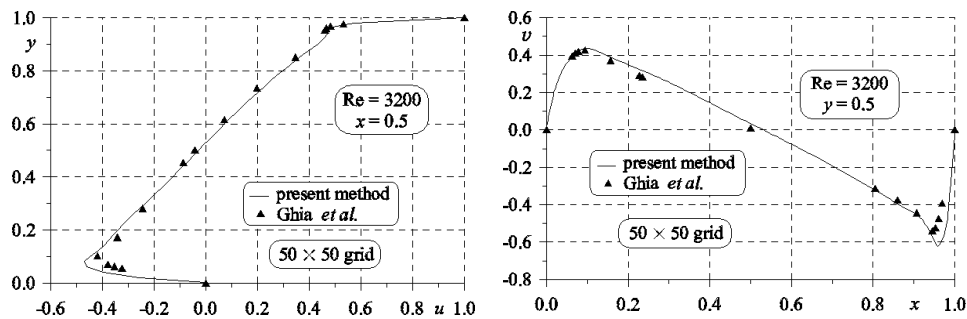

Figure 15. Distributions of the x and y components of velocity on the centrelines
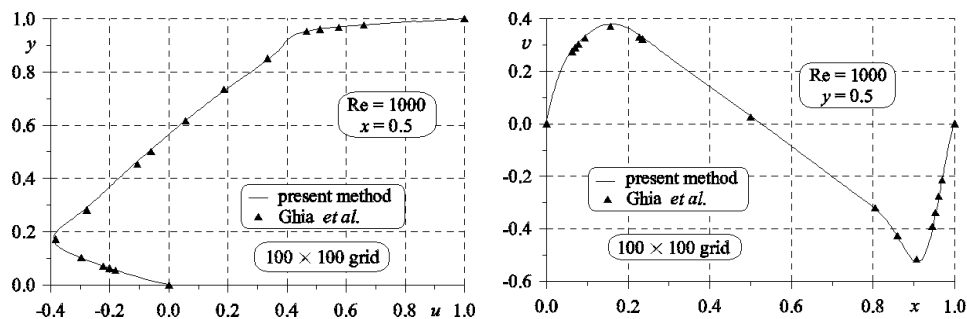of the cavity at $Re = 3200$, the 50×50 grid

Figure 16. Distributions of the x and y components of velocity on the centrelines
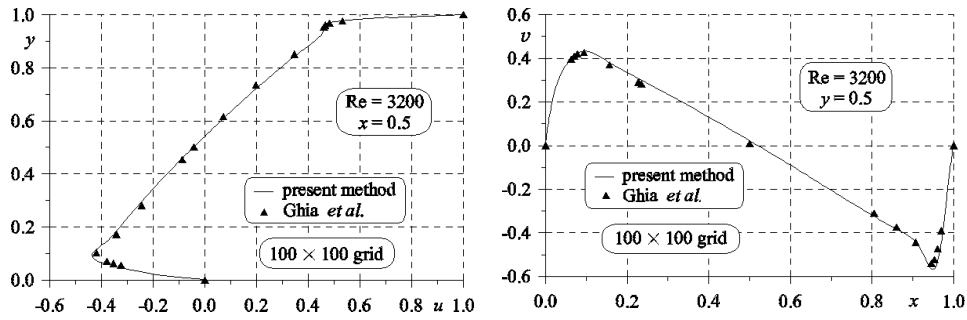of the cavity at $Re = 1000$, the 100×100 grid

Figure 17. Distributions of the x and y components of velocity on the centrelines
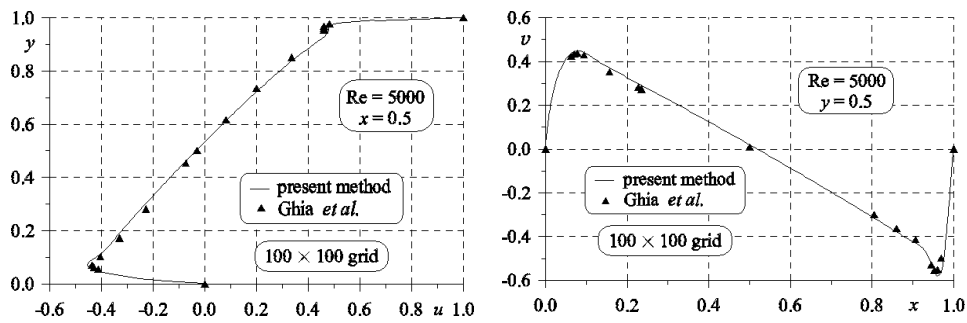of the cavity at $\mathrm{Re} = 3200$, the 100×100 grid

Figure 18. Distributions of the x and y components of velocity on the centrelines
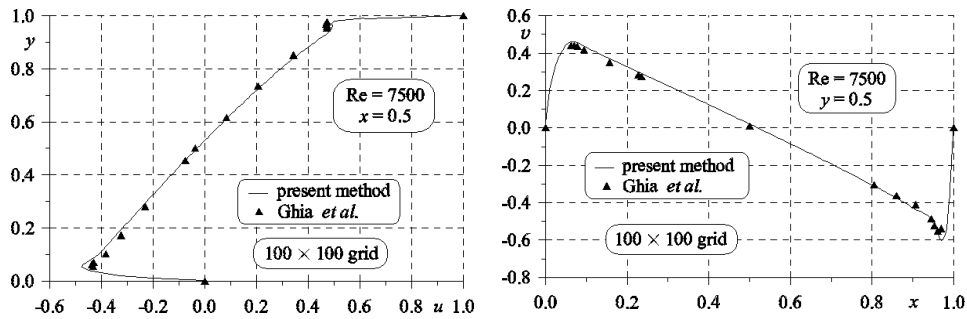of the cavity at $\mathrm{Re} = 5000$, the 100×100 grid

Figure 19. Distributions of the x and y components of velocity on the centrelines
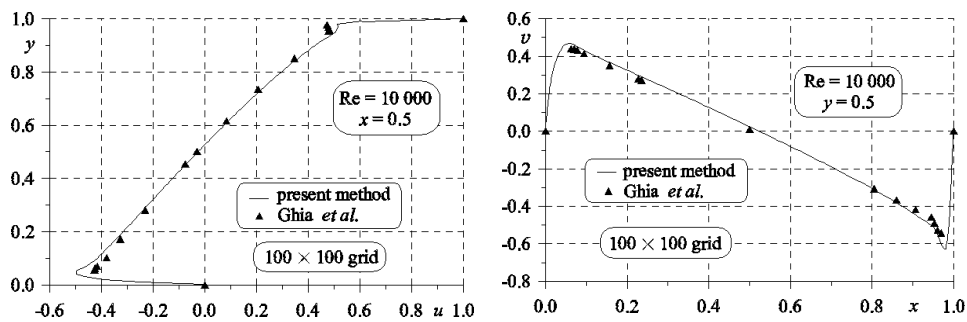of the cavity at $\mathrm{Re} = 7500$, the 100×100 grid

Figure 20. Distributions of the x and y components of velocity on the centrelines
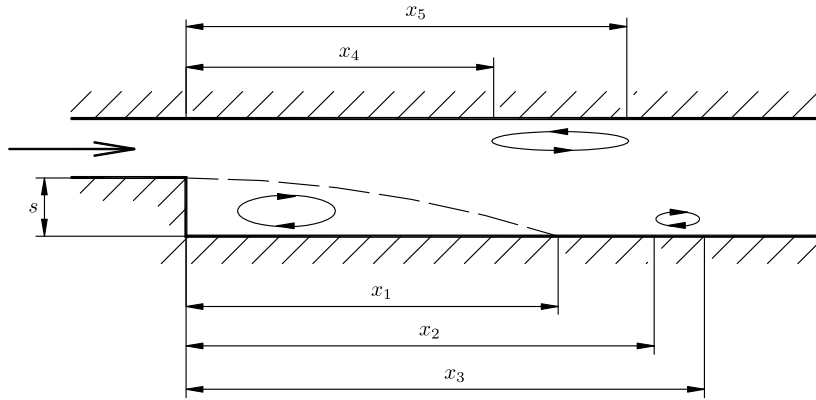of the cavity at $\mathrm{Re} = 10\,000$, the 100×100 grid

Figure 22. Re-circulation zones in the backward-facing step geometry

4.2. Numerical results

The assumed rectangular computational domain (Figure 21) on a uniform Cartesian $N \times M$ grid (8) can be discretized as follows:

$$x_i = ih, \quad y_j = -0.5 + jh, \tag{21}$$

where $h = 1/M$ is the identical grid size in the x and y directions, and indices i, j, $(0 \leq i \leq N, 0 \leq j \leq M)$ are related to the x and y directions, respectively.

By using the presented algorithm, computations were undertaken on the $30L \times 30$ grid (Equation (21)) and for channel lengths, L, within the range 10–30, with time steps $\Delta t = 1 \cdot 10^{-3}$ – Re = 200, $\Delta t = 5 \cdot 10^{-3}$ – Re = 400 and $\Delta t = 1 \cdot 10^{-2}$ – Re ≥ 600. Iterations ranging from 10 000 to 30 000 were necessary to achieve for laminar flows (Re ≤ 1200) with accuracy (19) within the range $[1 \cdot 10^{-8}, 1 \cdot 10^{-5}]$, while keeping the other calculation parameters same as in Section 3.2. Steady state solutions of this problem were obtained for Reynolds number values of 200, 400, 600, 800, 1200 and 2000 (see Figures 23–28).

Calculations according to the algorithm with second-order discretizations of the $\partial \vec{\nabla}^2 \psi / \partial t$ term and cubic spline function approximations of the spatial derivatives can be found in [49]. The computations were performed on $30L \times 30$ and $40L \times 40$ grids, $L = 20$ and $L = 25$, for Reynolds numbers Re ≤ 2500.

4.3. Comments on the results

The proposed algorithms have been proved to be also applicable as an incompressible Navier-Stokes solver for the numerical simulation of laminar and transitional motion of viscous incompressible fluids over a backward-facing step. The computed separation and reattachment points are in very good agreement with the numerical results reported in the literature. For example, the lengths of the re-circulation
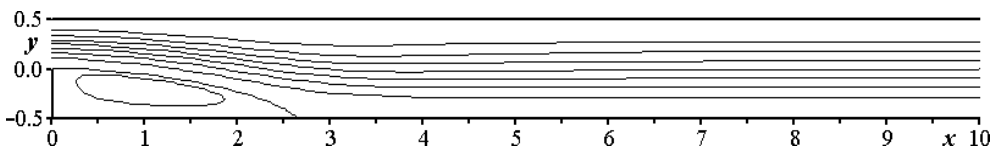

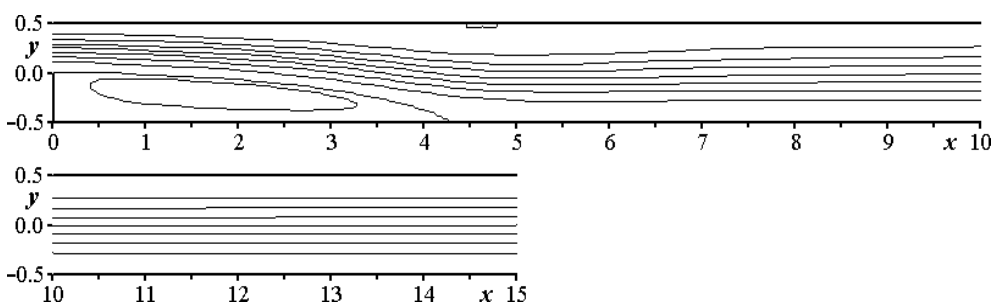**Figure 23.** Stream-function contours for Re = 200 on the 300×30 grid

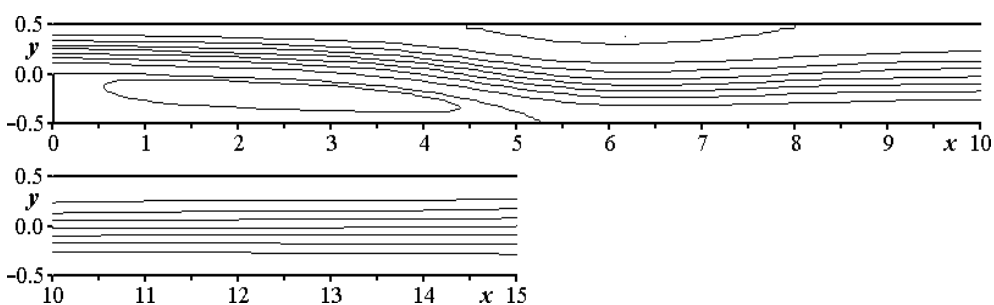**Figure 24.** Stream-function contours for Re = 400 on the 450 × 30 grid

Figure 25. Stream-function contours for Re = 600 on the 450 × 30 grid
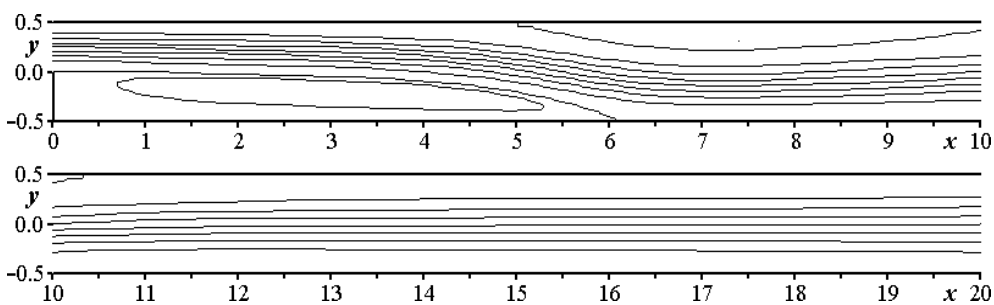

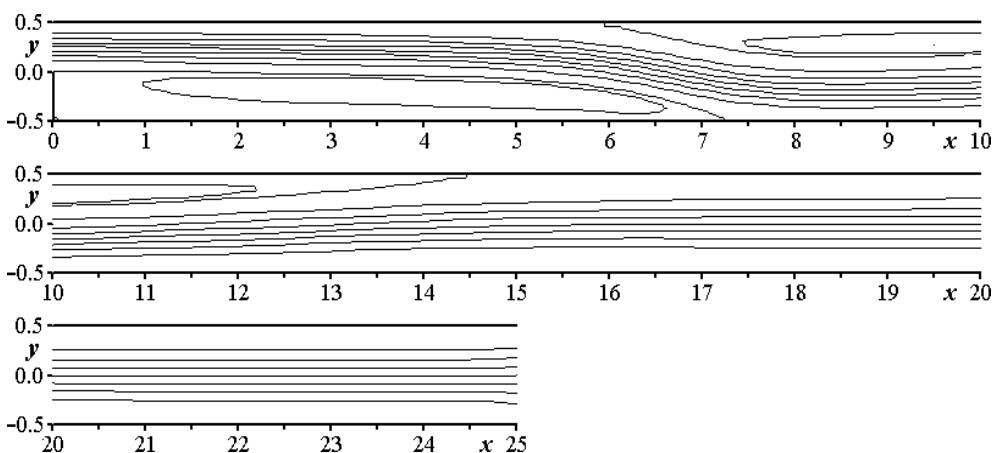**Figure 26.** Stream-function contours for Re = 800 on the 600 × 30 grid

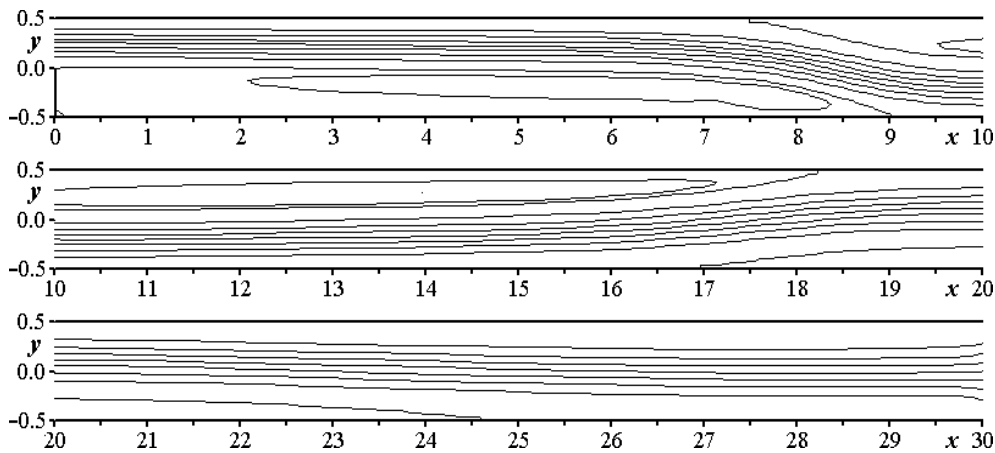**Figure 27.** Stream-function contours for Re = 1200 on the 750 × 30 grid

Figure 28. Stream-function contours for Re = 2000 on the 900 × 30 grid
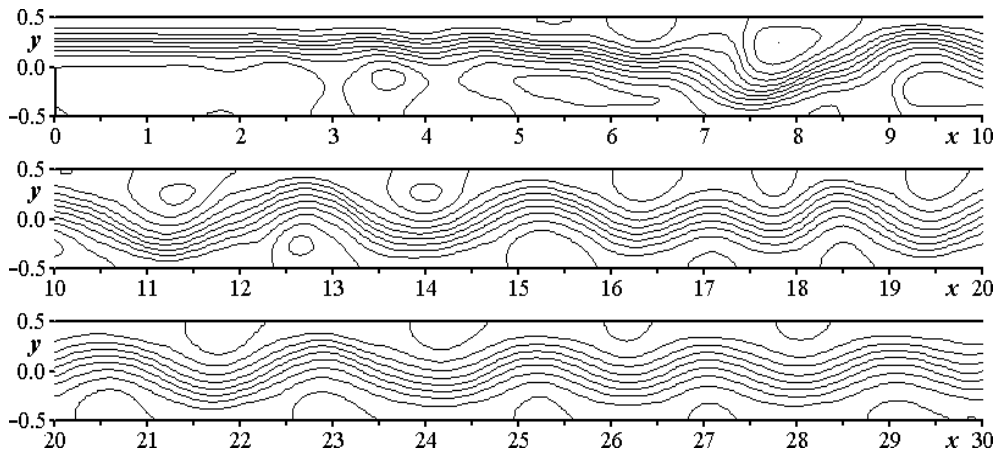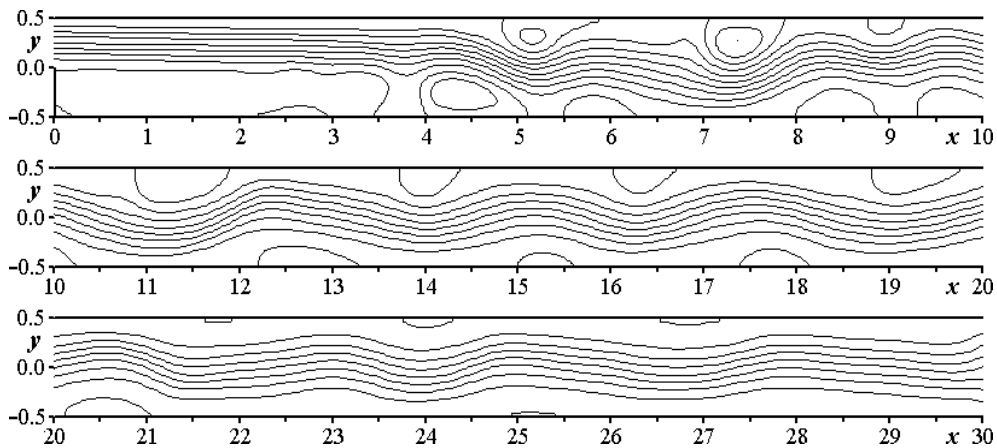

Figure 29. Stream-function contours for Re = 3000 on the 900 × 30 grid,
laminar inlet velocity profile

regions (Figure 22) obtained with the present method for Re = 800 are compared in
Table 1 with those reported by other authors.

In all the papers [50–73] computations have been performed for the $100 \leq$ Re $\leq$
800 laminar regime only, since it has been established that the flow is steady for
inlet Reynolds numbers up to Re = 800. The present calculations have shown that
the problem converges to a steady state solution for Re = 1200 (as already confirmed
by experimental results [50] and numerical calculations [49]) and for Re = 2000. The
calculations have indicated that flows over a backward-facing step become unsteady
and unstable for Reynolds numbers Re > 2000 (see Figure 29). Therefore, the choice of
proper boundary conditions for the inlet and outlet velocity profiles arises as another
important problem. The influence of inflow and outflow boundary conditions has been
studied by assuming experimentally determined turbulent velocity profiles in the inlet
as well as in the outlet channel [62]; the results are shown in Figure 30. At Re = 3000,
for both kinds of velocity profiles, the transient flow behind the backward-facing step
is composed of successive eddies generated along the lower and upper walls.

Table 1. Comparison of predicted separation and reattachment points for $Re = 800$

Authors	Grid	x_1	x_4	x_5
Gartling [51]	800×40	6.10	4.79	10.48
Pentaris *et al.* [52]	155×51	5.51	4.65	9.74
Pappou, Tsangaris [54]	150×31	6.10	4.87	10.37
Barton [55]	240×80	5.76	4.57	10.33
Barton [57]	80×50	6.10	4.82	10.45
Keskar, Lyn [58]	90×12	6.10	4.85	10.48
Domański, Kosma [66]	800×40	5.55	4.61	9.85
Kosma [49]	600×30	5.55	4.55	10.35
Kosma [49]	800×40	5.75	4.65	10.4
Present calculations (Figure 26)	600×30	6.1	5.0	10.3

Figure 30. Stream-function contours for $Re = 3000$ on the 900×30 grid, turbulent inlet and outlet velocity profiles

5. Concluding remarks

The developed computational algorithms for the solution of incompressible flow of viscous fluids substantially improve the previous versions proposed in papers [47–49]. The author is not aware of any other similar method for the solution of incompressible viscous flows; only in [7] a central difference scheme for a pure stream-function formulation of incompressible viscous flow was introduced. In their present form, the algorithms are applicable to numerical simulation of both laminar and turbulent motion as a solution of incompressible Navier-Stokes equations written in the form of a fourth-order equation for the stream function. The method of lines is adopted, the essence of which lies in discretizing all the spatial derivatives, while preserving the continuity of the time variable. The computed stream-function contours and distributions of velocity components in a wind-driven cavity and a rectilinear backward-facing step fit well the numerical results presented in numerous previously cited references. Because of their two-dimensionality, the present simulations are

limited to the unsteady flow regime and can be regarded as preliminary calculations for turbulent flow.

References

[1] Warsi Z U A 1993 *Fluid Dynamics: Theoretical and Computational Approaches*, CRC Press
[2] Roache P J 1998 *Computational Fluid Dynamics*, 2nd Edition, Albuquerque, Hermosa
[3] Lele S K 1992 *J. Comput. Phys.* **103** 16
[4] Kosma Z 2004 *Numerical Methods for Engineering Applications*, 2nd Edition, Radom University of Technology Publishing (in Polish)
[5] Hairer E, Norset S P and Wanner G 1987 *Solving Ordinary Differential Equations I: Nonstiff Problems*, Springer-Verlag
[6] Hairer E and Wanner G 1991 *Solving Ordinary Differential Equations II: Stiff and Differential-Algebraic Problems*, Springer-Verlag
[7] Kupferman R 2001 *SIAM J. Sci. Comput.* **23** 1
[8] Kumagai M 1982 *J. Comput. Phys.* **47** 130
[9] Ghia U, Ghia K N and Shin C T 1982 *J. Comput. Phys.* **48** 387
[10] Schreiber R and Keller H B 1983 *J. Comput. Phys.* **49** 310
[11] Kim J and Moin P 1985 *J. Comput. Phys.* **59** 308
[12] Kosma Z 1985 *Scientific Bulletin of Institute of Fluid-Flow Machinery of PAS*, Gdansk, **195/1133/85** (in Polish)
[13] Tanahashi T and Okanaga H 1990 *Int. J. Numer. Meth. Fluids* **11** 479
[14] Kovacs A and Kawahara M 1991 *Int. J. Numer. Meth. Fluids* **13** 403
[15] Huser A D and Biringen S 1992 *Int. J. Numer. Meth. Fluids* **14** 1087
[16] Ren G and Utnes T 1993 *Int. J. Numer. Meth. Fluids* **17** 349
[17] Sockol P H 1993 *Int. J. Numer. Meth. Fluids* **17** 543
[18] Li M, Tang T and Fornberg B 1995 *Int. J. Numer. Meth. Fluids* **20** 1137
[19] Churbanov A G, Pavlov A N and Vabishchevich P N 1995 *Int. J. Numer. Meth. Fluids* **21** 617
[20] Lee S-Ch and Chen Ch-K 1996 *Int. J. Numer. Meth. Fluids* **23** 47
[21] Chaviaropoulos P and Giannakoglou K 1996 *Int. J. Numer. Meth. Fluids* **23** 431
[22] Thomadakis M and Leschziner M 1996 *Int. J. Numer. Meth. Fluids* **22** 581
[23] Huang H and Seymour B R 1996 *Int. J. Numer. Meth. Fluids* **22** 713
[24] Weinan E and Liu J-G 1996 *J. Comput. Phys.* **126** 122
[25] Denero F M 1996 *Int. J. Numer. Meth. Fluids* **23** 125
[26] Zienkiewicz O C, Satya Sai B V K, Morgan K and Codina R 1996 *Int. J. Numer. Meth. Fluids* **23** 787
[27] Hadji S and Dhatt G 1997 *Int. J. Numer. Meth. Fluids* **25** 861
[28] Kosma Z 1999 *Determination of Laminar Incompressible Flows*, Monography of the Radom University of Technology (in Polish)
[29] Shankar P N and Deshpande M D 2000 *Annu. Rev. Fluid Mech.* **32** 93
[30] Jan Y J, Huang S J and Lee T Y 2000 *Int. J. Numer. Meth. Fluids* **34** 187
[31] Young D L, Yang S K and Eldho T I 2000 *Int. J. Numer. Meth. Fluids* **34** 627
[32] Guo D X 2000 *Appl. Numer. Math.* **35** 307
[33] Varonos A A and Bergeles G C 2001 *Int. J. Numer. Meth. Fluids* **35** 395
[34] Aydin M and Fenner R T 2001 *Int. J. Numer. Meth. Fluids* **37** 45
[35] Liu C H and Leung D Y C 2001 *Comput. Meth. Appl. Mech. Engrg.* **190** 4301
[36] Yan Y J 2002 *Int. J. Numer. Meth. Fluids* **39** 189
[37] Pan H and Damodaran M 2002 *Int. J. Numer. Meth. Fluids* **39** 441
[38] Auteri F and Parolini N 2002 *J. Comput. Phys.* **175** 1
[39] Mai-Duy N and Tran-Cong T 2003 *Int. J. Numer. Meth. Fluids* **41** 743
[40] Sahin M and Owens R G 2003 *Int. J. Numer. Meth. Fluids* **42** 57
[41] Sahin M and Owens R G 2003 *Int. J. Numer. Meth. Fluids* **42** 79
[42] Kalita J C, Dass A K and Dalal D C 2003 *Int. J. Numer. Meth. Fluids* **43** 1
[43] Eguchi Y 2003 *Int. J. Numer. Meth. Fluids* **41** 881

[44] Peng Y-F, Shiau Y-H and Hwang R R 2003 *Comput. Fluids* **32** 337
[45] Lin P, Guo Q and Chen X 2003 *Comput. Meth. Appl. Mech. Engng.* **192** 2555
[46] Zhang J 2003 *Comput. Math. Appl.* **45** 43
[47] Kosma Z 2001 *Scientific Bulletin of Chair of Applied Mechanics of Silesian University of Technology*, Gliwice **15** 179 (in Polish)
[48] Kosma Z 2002 *Scientific Bulletin of Chair of Applied Mechanics of Silesian University of Technology*, Gliwice **18** 201 (in Polish)
[49] Kosma Z 2003 *Numerical Simulation of Viscous Fluid Motions*, Monography of the Radom University of Technology (in Polish)
[50] Armaly B F, Durst F, Pereira J C F and Schönung B 1983 *J. Fluid Mech.* **127** 476
[51] Gartling D K 1990 *Int. J. Numer. Meth. Fluids* **11** 953
[52] Pentaris A, Nikolados K and Tsangaris S 1994 *Int. J. Numer. Meth. Fluids* **19** 1013
[53] Le T H, Troff B, Sagaut P, Dang-Train K and Ta Phuoc L 1997 *Int. J. Numer. Meth. Fluids* **24** 833
[54] Pappou Th and Tsangaris S 1997 *Int. J. Numer. Meth. Fluids* **25** 523
[55] Barton I E 1997 *Int. J. Numer. Meth. Fluids* **25** 633
[56] Biagioli F 1998 *Int. J. Numer. Meth. Fluids* **26** 887
[57] Barton I E 1998 *Int. J. Numer. Meth. Fluids* **28** 841
[58] Keskar J and Lyn D A 1999 *Int. J. Numer. Meth. Fluids* **29** 411
[59] Verma A K and Eswaran V 1999 *Int. J. Numer. Meth. Fluids* **30** 279
[60] Yee H C, Torczynski J R, Morton S A, Visbal M R and Sweby P K 2000 *Int. J. Numer. Meth. Fluids* **30** 675
[61] Brakkee E, Wesselin P and Kassels C G M 2000 *Int. J. Numer. Meth. Fluids* **32** 141
[62] Lenormand E, Sagaut P, Ta Phuoc L 2000 *Int. J. Numer. Meth. Fluids* **32** 369
[63] Barton I E and Kirby R 2000 *Int. J. Numer. Meth. Fluids* **33** 939
[64] Jan Y J, Huang S J and Lee T Y 2000 *Int. J. Numer. Meth. Fluids* **34** 187
[65] Kosma Z 2000 *Mech. Research Comm.* **27** 235
[66] Domański J and Kosma Z 2001 *Z. Angew. Math. Mech.* (ZAMM) **81** S4 921
[67] Whiting Ch H and Jansen K E 2001 *Int. J. Numer. Meth. Fluids* **35** 93
[68] Teigland R and Eliassen I K 2001 *Int. J. Numer. Meth. Fluids* **36** 519
[69] Olshanskii M A 2002 *Comput. Meth. Appl. Mech. Engng.* **191** 5515
[70] Pontaza J P and Reddy J N 2003 *J. Comput. Phys.* **190** 523
[71] Wan D C, Patnaik B S V and Wei G W 2002 *J. Comput. Phys.* **180** 229
[72] Sockol P M 2003 *J. Comput. Phys.* **192** 570
[73] Fernandez-Feria R and Sanmiguel-Rojas E 2004 *Comput. Fluids* **33** 463